Available online at www.sciencedirect.com
ScienceDirect
Icarus 194 (2008) 401–409
ICARUS
www.elsevier.com/locate/icarus

Global mapping of lunar crustal magnetic fields by Lunar Prospector

D.L. Mitchell [a,*], J.S. Halekas [a], R.P. Lin [a,b], S. Frey [a], L.L. Hood [c], M.H. Acuña [d], A. Binder [e]

[a] *Space Sciences Laboratory, University of California, Berkeley, CA 94720, USA*
[b] *Physics Department, University of California, Berkeley, CA 94720, USA*
[c] *Lunar and Planetary Laboratory, University of Arizona, Tucson, AZ 85721, USA*
[d] *NASA Goddard Space Flight Center, Greenbelt, MD 20771, USA*
[e] *Lunar Research Institute, Tucson, AZ 85747, USA*

Received 2 February 2007; revised 23 October 2007

Available online 12 January 2008

Abstract

The Lunar Prospector Electron Reflectometer has obtained the first global map of lunar crustal magnetic fields, revealing that the effects of basin-forming impacts dominate the large-scale distribution of remanent magnetic fields on the Moon. The weakest surface magnetic fields (<0.2 nT) are found within two of the largest and most recent impact basins, Orientale and Imbrium. Conversely, the largest concentrations of strong surface fields (>40 nT) are diametrically opposite to these same basins. This pattern is present though less pronounced for several other post-Nectarian impact basins larger than 500 km in diameter. The reduced strength and clarity of the pattern for older basins may be attributed to: (1) demagnetization from many smaller impacts, which erases antipodal magnetic signatures over time, (2) superposition effects from other large impacts, and (3) variation in the strength of the ambient magnetizing field. The absence of fringing fields stronger than 1 nT around the perimeter of the Imbrium basin or associated with craters within the basin implies that any uniform magnetization of the impact melt must be weaker than $\sim 10^{-6}$ G cm^3 g^{-1}. This limits the strength of any steady ambient magnetic field to no more than ~0.1 Oe at the lunar surface while the basin cooled for tens of millions of years following the Imbrium impact 3.8 billion years ago.

Keywords: Moon, surface; Magnetic fields; Cratering; Impact processes

1. Introduction

Remanent crustal magnetic fields are known to exist on Earth, Mars, and the Moon, and may exist on other terrestrial bodies in the Solar System. These fields provide a record of the magnetic environment at the time the rock last cooled below its Curie point (770 °C for metallic iron) or possibly was shock magnetized. On Earth, the study of crustal magnetism revealed polarity reversals of the core dynamo and confirmed the theory of plate tectonics (Vine and Matthews, 1963; Vine and Wilson, 1965; Pittman and Heirtzler, 1966). The remanent crustal fields at Mars provide striking evidence of a powerful dynamo and possibly tectonic activity that occurred early in that planet's history (Acuña et al., 1999; Connerney et al., 1999). Thermoremanent magnetization (TRM) in the presence of a dynamo field is the dominant process by which the terrestrial crust has been magnetized, and this is likely the case for Mars (Connerney et al., 1999). The origin of lunar magnetism is far less certain, and many hypotheses exist for the source of the ambient field and the magnetization process. Steady magnetizing fields of both external (solar or terrestrial) and internal (lunar dynamo) origin have been proposed, as have transient fields generated by impacts (for reviews, see Fuller, 1974, and Wieczorek et al., 2006). TRM is likely the dominant process for igneous lunar samples; however, shock remanent magnetization (SRM) may be significant in lightly metamorphosed breccias, which carry the strongest and most stable remanent magnetization of all lunar samples (Fuller et al., 1974; Fuller and Cisowski, 1987).

Today, the Moon has no global magnetic field ($<2 \times 10^{-8}$ of Earth's dipole moment; Russell et al., 1978); however, the Apollo missions discovered abundant evidence that magnetic fields once existed on the Moon. Magnetometers at the Apollo

* Corresponding author. Fax: +1 (510) 643 8302.
E-mail address: mitchell@ssl.berkeley.edu (D.L. Mitchell).

0019-1035/$ – see front matter
doi:10.1016/j.icarus.2007.10.027

landing sites measured fields as strong as 300 nT (1 nT $= 10^{-5}$ Gauss), and lunar rocks were found to carry remanent magnetization, implying ∼1-Oe surface fields between 3.6 and 3.9 billion years ago (Cisowski et al., 1983). (The oersted (Oe) is a unit of magnetic intensity (**H**) in a macroscopic medium, which is related to magnetic induction (**B**) by $\mathbf{B} = \mu\mathbf{H}$, where μ is the magnetic susceptibility of the medium. The magnetic susceptibility of the vacuum is unity.) Sub-micron grains of metallic iron are the dominant carriers of hard remanent magnetism in the lunar samples. These iron grains are produced from lunar minerals by impact processes in the highly reducing lunar environment, with a small contribution from metallic micrometeorites. Lunar soils and breccias contain a few tenths to 1% by weight of metallic iron, which is about ten times the metallic iron content of mare basalts (Nagata et al., 1972; Lucey et al., 2006). Consequently, soils and breccias are the most magnetic lunar materials, and terra samples are generally more magnetic than mare samples.

Magnetic field and electron reflection measurements obtained from the Apollo 15 and 16 subsatellites in 100-km-altitude orbits revealed hundreds of localized crustal magnetic fields, ranging in size from 7 km (the resolution limit) to ∼500 km across and having surface intensities up to hundreds of nanoteslas. Although these measurements were sparse and confined within ∼35° of the lunar equator, it was recognized that magnetic fields over the highlands are on average stronger than those over the maria (Coleman et al., 1972; Anderson et al., 1975; Lin, 1979), in accord with lunar sample measurements, and that the largest concentrations of strong crustal magnetic fields are located in zones diametrically opposite to the Imbrium, Serenitatis, Crisium, and Orientale impact basins (Lin et al., 1988).

The observed lunar magnetic fields arise from magnetization *contrasts* within the crust. Such contrasts may result from spatial variations in the abundance and/or type of magnetic carriers or by changes in the ambient magnetizing field when different crustal sources formed (e.g., impact melts and volcanic lavas). Subsequent impact disruption of the upper ∼10 km of the crust (Toksöz et al., 1973; Hörz et al., 1976; Cashore and Woronow, 1985) can modify existing magnetization contrasts and create new ones. The variety of possibilities often makes interpretation of orbital magnetic data difficult. For example, a magnetic anomaly associated with a fault or graben can be modeled equally well as leakage fields from a crack in a uniformly magnetized layer or as a magnetized subsurface dike (Srnka et al., 1979).

The correspondence of strong magnetic fields with the antipodal zones led to the hypothesis that crustal magnetization is associated with basin-forming impacts. According to this hypothesis, the hypervelocity (>10 km/s) impacts that form such large basins produce a plasma cloud that expands around the Moon, compressing and amplifying any pre-existing ambient magnetic field at the antipode (Hood and Huang, 1991). SRM associated with the focusing of seismic energy at the antipode and with basin ejecta impacting in the antipode region may occur (Hood and Artemieva, 2008). Peak shock pressures are calculated to exceed 2 GPa for the convergence of seismic waves (Watts et al., 1991) and 10 GPa for impacts (Hood and Vickery, 1984), sufficient for acquisition of SRM (Fuller et al., 1974). A key element of this hypothesis is that any ambient magnetic field is greatly amplified at the antipode, where magnetization takes place, thus eliminating the need for a strong pre-existing field. Nevertheless, the four impacts that correspond to the strongest antipodal magnetic fields occurred from 3.9 to 3.7 billion years ago (Stoffler and Ryder, 2001), at about the same time that the most strongly magnetized Apollo samples were formed (Cisowski et al., 1983), suggesting an epoch of relatively strong ambient magnetic fields.

2. Observations and data analysis

After entering a polar orbit around the Moon in January 1998, the Lunar Prospector (LP) spacecraft returned the first new data on lunar magnetic fields in twenty-six years (Lin et al., 1998). The Magnetometer/Electron Reflectometer (MAG/ER) experiment onboard LP was designed to map crustal magnetic fields over the entire surface. The MAG detects perturbations caused by crustal sources to the ambient field at the spacecraft, which yields a vector measurement with a spatial resolution comparable to the spacecraft altitude and a sensitivity that depends strongly on distance from the source. The ER measures the pitch angle distributions of electrons reflected from crustal magnetic fields to infer the surface field strength with a sensitivity (∼0.2 nT) and spatial resolution (∼5 km) that are independent of spacecraft altitude.

Electron reflection magnetometry makes use of the magnetic mirror effect. In a uniform magnetic field an electron travels in a helical trajectory with a constant pitch angle (α) between the particle's velocity and the magnetic field (Fig. 1). If the field varies spatially and the fractional change in the field is small over the distance traveled by an electron in one gyration, then the kinetic energy ($W = mv^2/2$) and magnetic moment ($\mu = mv_\perp^2/2B$) are conserved, and the particle's pitch angle changes such that $|\mathbf{B}|/\sin^2\alpha = \text{constant}$. If the pitch angle of a downward traveling particle reaches 90° before it impacts the surface, it is reflected back up to the spacecraft; otherwise, it is absorbed. The cutoff pitch angle, α_c, is defined as $|\mathbf{B}_{sc}|/\sin^2\alpha_c = |\mathbf{B}_{surf}|$, where $\mathbf{B}_{sc}$ and $\mathbf{B}_{surf}$ are the magnetic fields at the spacecraft and surface, respectively. Estimates of $|\mathbf{B}_{surf}|$ are obtained by combining measurements of $\mathbf{B}_{sc}$ and α_c at the spacecraft.

The LP electron reflection data were obtained at lower energies (220–520 eV) than the Apollo subsatellite data (0.5 and 14 keV), and we found it necessary to correct the LP measurements for electrostatic reflection caused by differential charging of the lunar surface and the LP spacecraft (Halekas et al., 2002b). If the electron motion remains adiabatic, then the expression for energy conservation becomes $W = mv^2/2 + eU$, where e is the electron charge, and U is the electrostatic potential. The expression for the surface magnetic field strength is then:

$$|\mathbf{B}_{surf}| = (1 - e\Delta U/E)|\mathbf{B}_{sc}|/\sin^2\alpha_c,$$

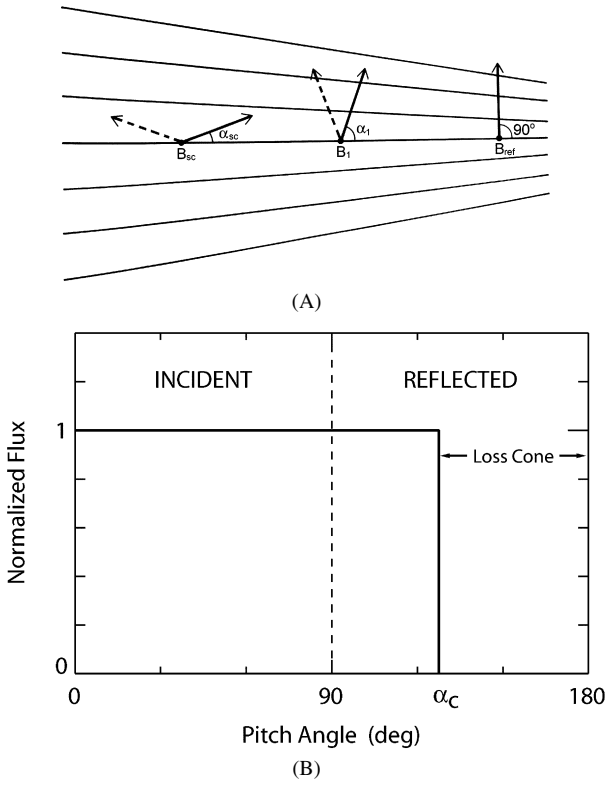

Fig. 1. (A) Instantaneous velocity vectors for an electron traveling along converging magnetic field lines between the spacecraft and the reflection point (solid: incident, dashed: reflected). As the electron travels towards increasing magnetic field strength, its pitch angle (α) satisfies $B/\sin^2\alpha = \text{constant}$. The electron is reflected back towards the spacecraft when α reaches 90°, and $B_{\text{ref}} = B_{\text{sc}}/\sin^2\alpha_{\text{sc}}$. (B) Electron pitch angle distribution measured at the spacecraft. For the Moon, the loss cone is formed at the surface, resulting in a sharply defined cutoff pitch angle (α_c).

where ΔU is the potential difference between the surface and the spacecraft (typically -35 V on the lunar night side), and E is the electron energy measured at the spacecraft. We solve for both $|\mathbf{B}_{\text{surf}}|$ and ΔU by measuring α_c at different energies (220, 340, and 520 eV). Monte Carlo simulations show that this is possible when the surface magnetic field strength is between ~0.2 and 10 nT. For stronger surface fields, the effect of the potential drop is small compared with measurement errors, and we can safely ignore the electric field correction.

The surface magnetic field is the vector sum of the crustal field ($\mathbf{B}_c$) and the external (interplanetary or geomagnetic) field, which to a good approximation is the field measured at the spacecraft ($\mathbf{B}_{\text{sc}}$). If we represent the crustal field with a dipole, for example, then the surface field strength is greatest when this dipole is parallel to the external field. Other orientations of the dipole result in weaker surface fields; however, the crustal field is still detectable even when the dipole is antiparallel to the external field, since the field line passing through the spacecraft will map to nearby regions around the dipole, where $|\mathbf{B}_{\text{surf}}| > |\mathbf{B}_{\text{sc}}|$. Thus, without knowledge of the orientation of the crustal field, a lower bound to its strength is given by $|\mathbf{B}_c| \geqslant |\mathbf{B}_{\text{surf}}| - |\mathbf{B}_{\text{sc}}|$, which we adopt as a reasonable first approximation to $|\mathbf{B}_c|$ (see Lin et al., 1976).

Estimates of $|\mathbf{B}_c|$ are mapped onto the lunar surface by extrapolating the magnetic field vector at the spacecraft in a straight line until it intersects the Moon. The spatial resolution at the surface is set by the diameter of the electron's helical path, which is ~5 km at 300 eV. The straight line approximation typically introduces mapping errors comparable to or smaller than this resolution, except near the strongest crustal fields, where the error approaches ~30 km (Delory et al., 2002). The ER measures surface field strengths up to ~250 nT, beyond which α_c becomes too small to be resolved by the instrument. Over the 18-month LP mission, the ER obtained 7×10^5 electron reflection measurements distributed around the entire Moon, which yielded 1.5×10^5 estimates of $|\mathbf{B}_c|$, corrected for electrostatic charging. These data have previously been used to produce regional maps of the lunar near side (Halekas et al., 2001), lunar impact craters (Halekas et al., 2002a), and the Imbrium and Serenitatis antipodes (Lin et al., 1998). Here, we present a global map of the lunar surface magnetic field and interpret the large-scale distribution of magnetic sources.

3. Small-scale magnetic anomalies

The ER was designed to measure a pitch angle distribution every 2.5 s, during which time the spacecraft moves 4 km in its orbit, thus allowing for complete sampling in latitude at the ER's intrinsic spatial resolution. During a typical orbit over highland terrain, many isolated magnetic anomalies are observed with $|\mathbf{B}_c|$ ranging from a few to more than 100 nT (Fig. 2). Some of these anomalies have dimensions of only 10 km along the orbit track, which is close to the resolution limit. Nearby orbit tracks (Fig. 3) indicate that a similar scattered distribution occurs in longitude, although adjacent orbits are spaced by 1° (~30 km at the equator). Significant magnetic field variations were observed on even smaller scales along LRV traverses at the Apollo 14 and 16 landing sites (Dyal and Parkin, 1972).

Although the ER technique provides no polarity information for the crustal field, the small scale sizes and scattered distribution of magnetic intensity features suggest that the magnetic sources that give rise to the observed field lack coherence. This could be explained if most of the observable magnetic sources exist in a relatively shallow layer (~0–10 km) that has been vulnerable to impact disruption, but does not rule out the possibility of a uniform magnetization at greater depths, which would produce no detectable fields at the surface. However, the presence of such a layer can be revealed by the demagnetization signatures of impact craters larger than ~10 km in diameter, since a hole in a uniformly magnetized layer results in an external fringing field. The absence of fringing fields in the demagnetization signatures of impact craters larger than 50 km in diameter (Halekas et al., 2002a) implies that no significant magnetization with coherence scales greater than ~25 km exists in the upper few tens of kilometers of the lunar crust. Since even deeper layers approach the Curie isotherm for metallic iron (Hood, 1986), these results indicate that any large-scale uniform magnetization preserved within the crust is insignif-

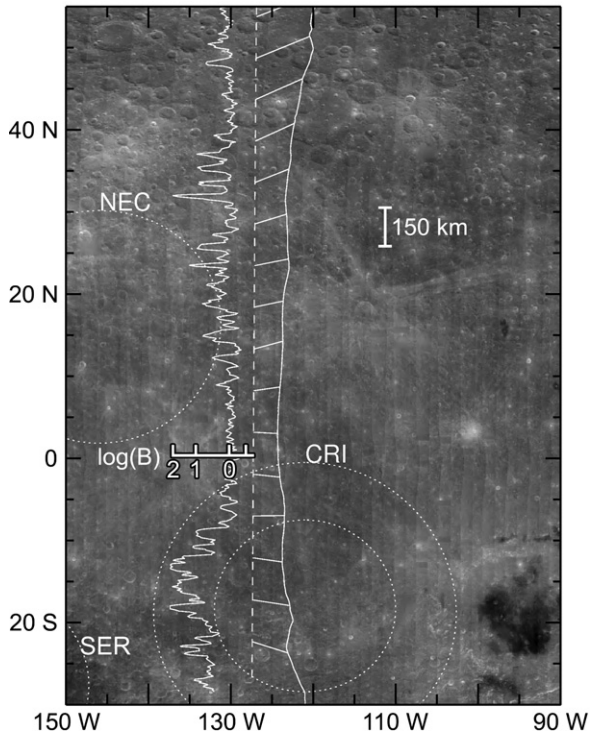

Fig. 2. A trace of the surface crustal magnetic field strength ($|\mathbf{B}_c|$) obtained from 10:03 to 10:30 UT on 4 Sept. 1998 reveals numerous small-scale anomalies. The Moon was in a geomagnetic tail lobe (geocentric solar ecliptic (GSE) longitude of 152°) and the spacecraft was on the night hemisphere. The dashed line shows the orbit of Lunar Prospector as it moves southward, 100 km above the lunar surface. The solid curve to the right of the orbit is the locus of points on the surface where the magnetic field passing through the spacecraft intersects the Moon (some of these field lines are shown as "ladder rungs")—these are the reflection points for electrons measured at the spacecraft. The variable quantity to the left of the orbit is an estimate of the surface magnetic field intensity. Dotted circles are antipodal to the main rims of the Crisium (CRI, largest interior ring also shown), Nectaris (NEC), and Serenitatis (SER) impact basins. The background image is from Clementine data (http://www.nrl.navy.mil/clementine/clib).

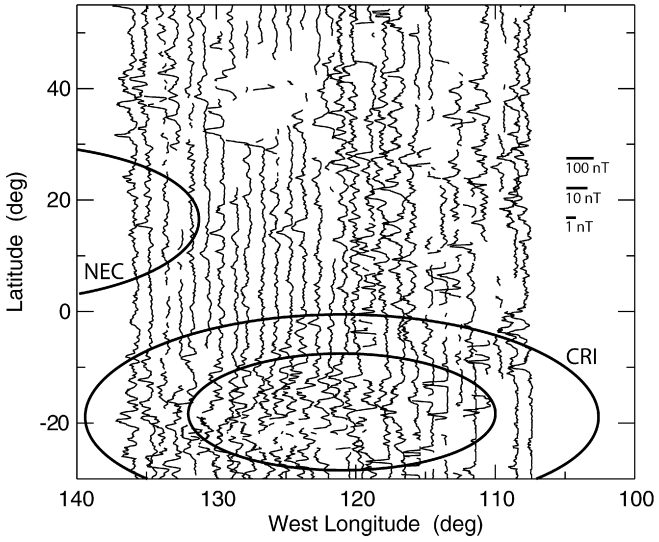

Fig. 3. Traces of the surface crustal magnetic field strength ($|\mathbf{B}_c|$) obtained on 27 consecutive orbits (18–21 March 1999). The Moon was in the solar wind upstream of Earth's bow shock (GSE longitudes of 8°–48°), and the spacecraft was on the night hemisphere. Orbit tracks are spaced by 1° in longitude (~30 km at the equator), and surface reflection points are omitted for clarity. Gaps in the traces (e.g., the region centered near 127° W, 38° N) are caused by loss of magnetic connectivity to the lunar surface, and to a lesser extent, data gaps. In some cases, magnetic features can be seen at nearly the same latitude on 2–3 consecutive orbits (e.g., 125° W, 15° N). Note the relatively high surface field strengths within and northeast of the Crisium antipode. These trends can be seen in Fig. 4.

icant compared with the magnetization that gives rise to the observed small-scale magnetic fields.

4. Global distribution of surface magnetic fields

Even with 1.5×10^5 measurements, the orbit spacing in longitude is insufficient over much of the Moon to produce a fully sampled map at the intrinsic resolution. (With a resolution of 5 km, $>2 \times 10^6$ measurements would be required to fully sample the lunar surface.) Traces of the surface magnetic field strength obtained on many consecutive orbits (Fig. 3) clearly show large-scale trends. For example, surface fields are systematically high within the Crisium antipode (see Table 1 for locations of impact basins), and there is a relatively high concentration of magnetic features northeast of that antipode. To reveal large-scale trends in the surface magnetic field, we average the data in 5 × 5-degree bins (Fig. 4). The most prominent feature at this resolution is a region of strong (>40 nT) surface fields diametrically opposite to the Imbrium and Serenitatis impact basins. This is the same region that was partially mapped northward of 35° S by the Apollo subsatellites (Anderson et al., 1975; Lin, 1979). The LP data show that strong surface magnetic fields extend to the southern-most regions of the antipodal zones, while increasing the number of measurements in the region more than tenfold.

Conversely, the largest concentration of weak surface fields (<0.2 nT) is located within the Imbrium basin itself (Figs. 4 and 5). These fields are several times weaker than typical fields over other maria. Two prominent magnetic anomalies in southeastern Oceanus Procellarum, Reiner Gamma (59° W, 7° N) and Rima Sirsalis (60° W, 14° S), show evidence that the magnetized material that gives rise to these anomalies is buried beneath surficial mare deposits (Hood et al., 2001; Hood et al., 1979; Anderson et al., 1977). The mare lavas are only a few kilometers thick (Williams and Zuber, 1998; Wieczorek et al., 2006), whereas the underlying crust above the Curie isotherm is tens of kilometers thick (Hood, 1986). Furthermore, the remanent magnetizations of igneous lunar samples are typically an order of magnitude weaker than those of breccias. Thus, it is reasonable to expect that the very low fields over Mare Imbium result primarily from a lack of magnetization contrasts beneath the lava.

The Imbrium impact would have destroyed any pre-existing magnetization of the target material, either thermally or by shock. When the impact melt subsequently cooled through the Curie point, it would have acquired TRM if an ambient magnetic field were present. This magnetization could be revealed by leakage fields associated with later impacts within the basin or by a fringing field around the basin perimeter. Most craters

Table 1
Lunar impact basins[a]

	Basin name	Age group[b]	Age (Gyr)[c]	Center		Diameter (km)[d]	B_o (nT)[e]
				Lat.	Long.		
1.	Orientale	1-I	3.72–3.85?	20° S	95° W	930	100
2.	Schrödinger	2-I		75° S	134° E	320	100
3.	Imbrium	3-I	3.75–3.87	33° N	18° W	1200–1500	100
4.	Sikorsky–Rittenhouse	4-N		69° S	111° E	310	50
5.	Bailly			67° S	68° W	300	50
6.	Hertzsprung			2° N	129° W	570	50
7.	Serenitatis		3.84–3.90	27° N	19° E	740	50
8.	Crisium		3.80–3.91	18° N	59° E	635	50
9.	Humorum			24° N	40° W	440	50
10.	Humboldtianum			61° N	84° E	600	50
11.	Mendeleev	5-N		6° N	141° E	330	25
12.	Mendel–Rydberg	6-N		50° S	94° W	460	25
13.	Korolev			5° S	157° W	440	25
14.	Moscoviense			26° N	147° E	445	25
15.	Nectaris		3.80–3.95	16° S	34° E	860	25
16.	Apollo	7-pN		36° S	151° W	505	10
17.	Grimaldi			5° S	68° W	430	10
18.	Freundlich–Sharonov	8-pN		19° N	175° E	600	10
19.	Birkhoff	9-pN		59° S	147° W	330	10
20.	Planck			58° S	136° E	325	10
21.	Schiller–Zucchius			56° S	45° W	325	10
22.	Amundsen–Ganswindt			81° S	120° E	355	10
23.	Lorentz	10-pN		34° N	97° W	360	10
24.	Smythii	11-pN		2° S	87° E	840	10
25.	Coulomb–Sarton			52° N	123° W	400	10
26.	Keeler–Heaviside	12-pN		10° S	162° E	540	10
27.	Poincaré			58° S	162° E	340	10
28.	Ingenii			34° S	163° E	325	10
29.	Lomonosov–Fleming	13-pN		19° N	105° E	620	10
30.	Nubium			21° S	15° W	690	10
31.	Fecunditatis			4° S	52° E	690	10
32.	Mutus–Vlacq			52° S	21° E	700	10
33.	Tranquillitatis			7° N	40° E	775	10
34.	Australe			52° S	95° E	880	10

[a] Adapted from Wilhelms (1984).
[b] Although the chronology of lunar impact basins is uncertain, they can be reliably placed into 13 age groups (I = Imbrian, N = Nectarian, pN = pre-Nectarian). Basins are numbered in the reverse order of the impact sequence in our model.
[c] Age estimates are from Stoffler and Ryder (2001).
[d] Diameter listed is that of the largest confidently identified ring.
[e] Normalization of our model, which is based on lunar sample measurements (see text).

within the basin (ranging from 10 to 90 km in diameter) show no evidence for leakage fields stronger than ∼0.2 nT at the surface. Our ability to detect a fringing field around the basin perimeter is complicated by the possible presence of small-scale magnetization contrasts just beyond the perimeter that survived the impact. However, most surface fields within 0.5 basin radii of the main rim, particularly to the west, are weaker than ∼1 nT (Fig. 4), which provides a useful upper bound on the strength of the fringing field.

The absence of surface fields stronger than ∼1 nT within or around the Imbrium basin places limits on the magnetization of the impact melt. If the melt volume is 100 times larger than the impactor volume (Orphal et al., 1980) and if the impactor diameter is 20 times smaller than the basin diameter (Chapman and Morrison, 1994), then the thickness of impact melt spread uniformly within the basin would be of order 1% of the basin diameter. This translates to ∼10 km for Imbrium, which is too thick to have been significantly demagnetized by the heat of later lava flows over the basin. The magnetization of this disk must be weaker than $\sim 10^{-6}$ G cm^3 g^{-1} to avoid fringing fields stronger than 1 nT.

If we assume that the ambient field remained steady while the impact melt cooled and that the ability of the recrystallized melt to carry hard magnetic remanence is no less than that of igneous Apollo samples, then the strength of the ambient field at the time of the Imbrium impact could have been no more than ∼0.1 Oe. A wide range of paleofield strengths, mostly stronger than 0.1 Oe, was apparently required to magnetize the Imbrium-era Apollo samples (Cisowski et al., 1983). If the ambient field was due to a lunar core dynamo, then several polarity reversals could have occurred during the tens of millions of years required for the impact site to cool below the Curie temperature (Bratt et al., 1985). This could account for the weak surface fields within and around Imbrium and for the variable paleofield

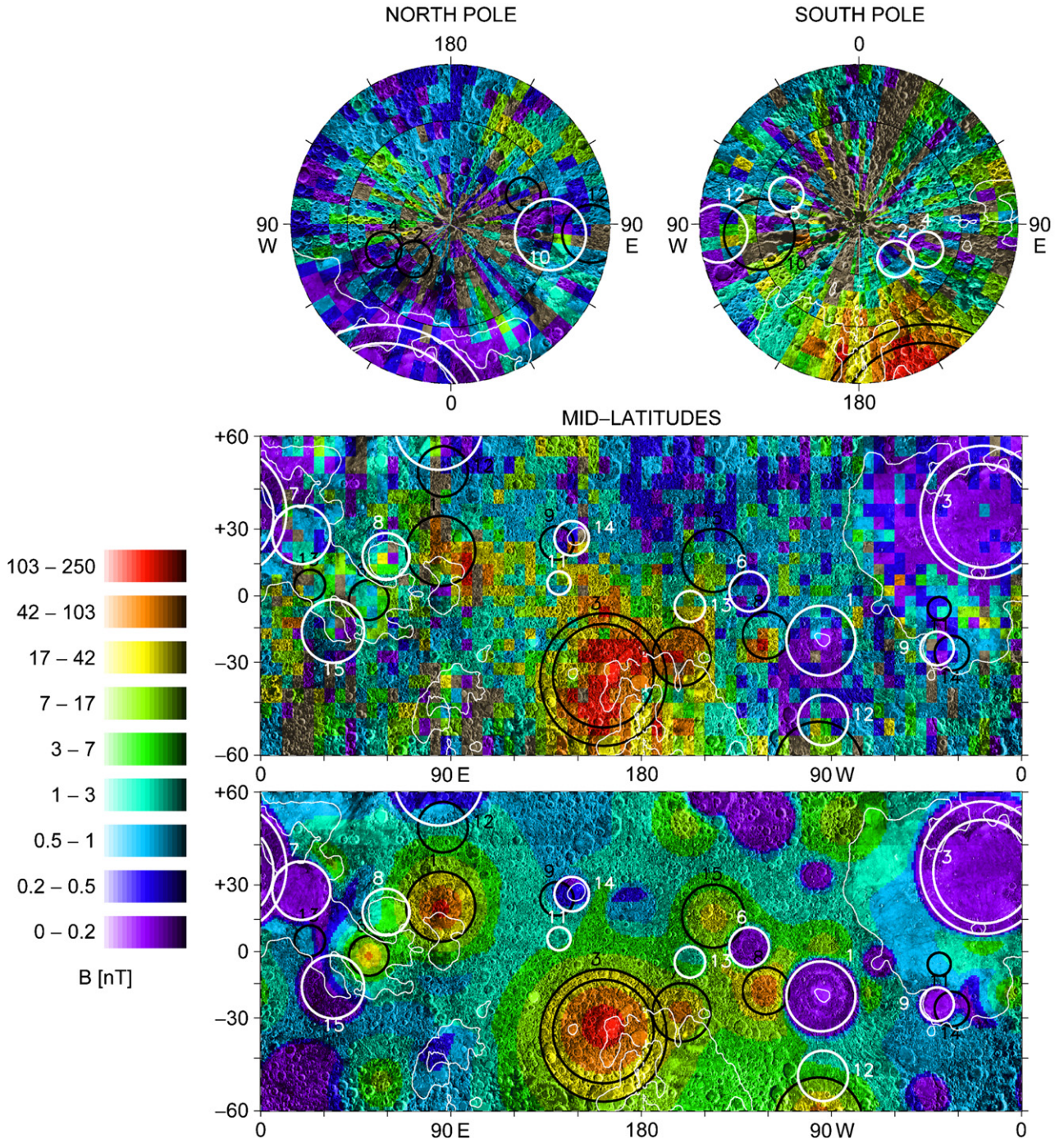

Fig. 4. Colors representing the surface crustal magnetic field intensity ($|\mathbf{B}_c|$) are superimposed onto a shaded relief map of the Moon (circles and upper panel). The data included in this image consist of ∼150,000 measurements, each with a spatial resolution of 5 km. These are binned into 5 × 5-degree elements (1 deg = 30 km at the equator), and the mean field strength within each element is color-coded. An optical albedo contour separates maria from highlands. White circles mark the main rims of the 15 most recent lunar impact basins (numbered according to Table 1; for Imbrium, the largest interior ring is also shown). Black circles are antipodal to white circles. An empirical model (bottom panel) is constructed by sequentially applying the magnetizing and demagnetizing effects of all known basin-forming impacts.

strengths inferred from sample measurements. If SRM is an important process on the Moon, then other variable factors, such as ambient magnetic field amplification and shock pressure, could have also played a role.

The pattern of weak magnetic fields at the impact site and strong fields at the antipode is also clearly seen for the Orientale basin. At ∼3.8 billion years old, Orientale and Imbrium are two of the last three basin-forming impacts on the Moon (Table 1), and are thus least subject to superposition effects. Two older basins, Crisium and Serenitatis, show clear antipodal magnetic enhancements, but the corresponding basins are not strongly demagnetized. The Crisium basin could have been remagnetized because of its proximity to the younger Orientale and Hertzsprung antipodes. In addition, there is evidence

that some magnetized Imbrium ejecta were emplaced within about two basin radii from the impact site. The Reiner Gamma and Rima Sirsalis magnetic anomalies are highly elongated and nearly radially aligned with the center of the Imbrium basin, suggesting that both arise from buried ejecta (e.g., Hood et al., 2001). In addition, magnetic anomalies south of the Imbrium basin (Fig. 4) are correlated with Cayley deposits (Halekas et al., 2001), which are thought to be ejecta from the Imbrium impact. Such "near-field" magnetization might account for fields within the Serenitatis basin.

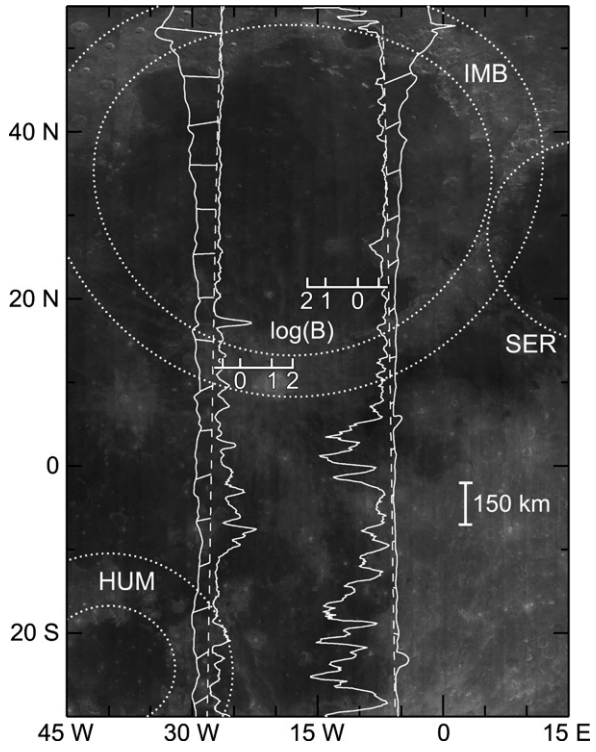

Fig. 5. Representative traces of the surface crustal magnetic field strength ($|\mathbf{B}_c|$) over the Imbrium basin. Both traces were obtained while the Moon was in the solar wind and the spacecraft was on the night hemisphere (left: 15:16–15:42 UT on 21 July 1999; right: 2:53–3:18 UT on 19 March 1999). The surface field strength is below the detection threshold (~0.2 nT) over much of the basin, although a few isolated anomalies are present. Note the much stronger surface fields south of the Imbrium basin. Dotted circles are the main rims (*not* antipodes) of the Imbrium (IMB), Serenitatis (SER), and Humorum (HUM) impact basins.

5. Monte Carlo simulation

The antipodal magnetic enhancements of the four largest post-Nectarian basins (Imbrium, Orientale, Serenitatis, and Crisium) suggest that a significant component of lunar magnetism is associated with large impacts, either by magnetization of the antipodal crust, or by the emplacement of magnetized material preferentially at the antipode. Could this apparent association have occurred by chance? To address this question, we took the observed surface magnetic field distribution as fixed and randomly relocated the antipode rings of all basins younger than Nectaris and larger than 500 km in diameter. For each random placement of these antipodes, we determined the mean field strength inside each ring, ordered them from strongest to weakest mean field strength, and compared these to the observed values (Table 2). There is a 6% chance of obtaining a mean field of at least 58.7 nT for any one of these randomly placed rings, while the likelihood of obtaining significant magnetic enhancements within two or more rings is much less. There is only a 0.02% chance of randomly obtaining significant magnetic en-

Table 2
Monte Carlo results (Imbrium antipode included)

Criteria[a]	All cases (out of 10^7)	Non-overlapping cases[b] (out of 3,555,720)
$\mathbf{B}_1 \geqslant 58.7$ nT	607,369	221,694
and $\mathbf{B}_2 \geqslant 23.8$ nT	127,802	20,479
and $\mathbf{B}_3 \geqslant 18.2$ nT	20,627	1379
and $\mathbf{B}_4 \geqslant 8.4$ nT	5687	188
and $\mathbf{B}_5 \geqslant 4.2$ nT	**2356**	**51**
and $\mathbf{B}_6 \geqslant 2.4$ nT	1425	25
and $\mathbf{B}_7 \geqslant 2.4$ nT	355	5

[a] B_N is the average surface magnetic field strength within one basin radius of the antipode of basin N (ordered by decreasing field strength). The observed values of B_N are: Imbrium (58.7 nT), Serenitatis (23.8 nT), Orientale (18.2 nT), Crisium (8.4 nT), Nectaris (4.2 nT), Hertzsprung (2.4 nT), and Humboldtianum (2.4 nT). The mean surface field strength in the non-antipodal highlands is 3.0 nT.

[b] No two basin antipodes overlap, as for the seven actual basins.

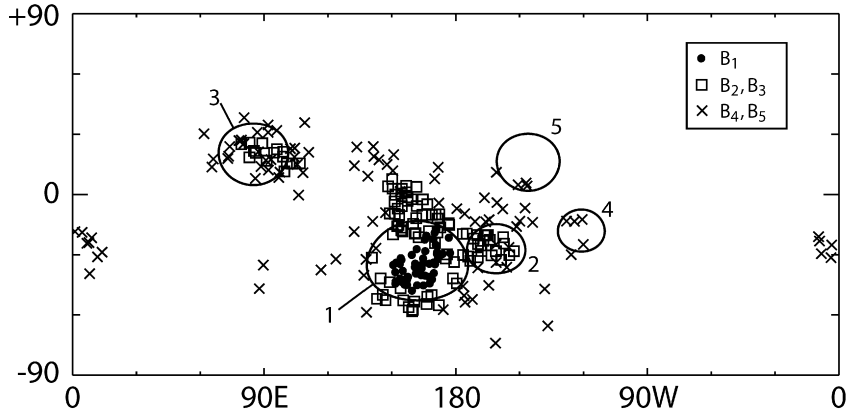

Fig. 6. Antipode center locations for the 51 non-overlapping random cases for which the five greatest mean antipodal field strengths meet or exceed the observed values (see Table 2). Numbered circles show the actual antipode locations of all basins younger than Nectaris and larger than 500 km in diameter. Antipode circles are numbered as they are identified in Table 1.

Table 3
Monte Carlo results (Imbrium antipode excluded)

Criteria[a]	All cases (out of 10^7)	Non-overlapping cases[b] (out of 5,575,685)
$\mathbf{B}_1 \geqslant 23.8$ nT	687,451	389,028
and $\mathbf{B}_2 \geqslant 18.2$ nT	70,274	27,095
and $\mathbf{B}_3 \geqslant 8.4$ nT	19,054	4680
and $\mathbf{B}_4 \geqslant 4.2$ nT	**8241**	**1630**
and $\mathbf{B}_5 \geqslant 2.4$ nT	4900	888
and $\mathbf{B}_6 \geqslant 2.4$ nT	1181	181

[a] B_N is the average surface magnetic field strength within one basin radius of the antipode of basin N (ordered by decreasing field strength). The observed values of B_N are: Imbrium (58.7 nT), Serenitatis (23.8 nT), Orientale (18.2 nT), Crisium (8.4 nT), Nectaris (4.2 nT), Hertzsprung (2.4 nT), and Humboldtianum (2.4 nT). The mean surface field strength in the non-antipodal highlands is 3.0 nT.
[b] No two basin antipodes overlap, as for the seven actual basins.

hancements within 5 of the 7 rings, and if we further insist that none of the seven rings overlap, as observed, then the odds drop to 0.0014%.

The distribution of antipode centers for the 51 non-overlapping Monte Carlo runs for which the five greatest mean antipodal field strengths meet or exceed the observed values is shown in Fig. 6. The ring with the largest enhancement ($\geqslant$58.7 nT) is always centered within the Imbrium antipode, while the rings with the second and third largest enhancements ($\geqslant$23.8 and $\geqslant$18.2 nT) tend to be located within the Orientale and Serenitatis antipodes, or in the vicinity of the Imbrium antipode (especially to the north). The rings with the fourth and fifth largest enhancements ($\geqslant$8.4 and $\geqslant$4.2 nT) are more scattered, since these enhancements are not much greater than the mean highland field outside of the post-Nectarian antipodes (3 nT).

Similar results are obtained if we mask all magnetic fields within the Imbrium antipodal ring and repeat the Monte Carlo analysis for the other six rings (Table 3). We conclude that it is extremely unlikely that the observed magnetic enhancements within the five largest post-Nectarian basin antipodes occurred by chance. Antipodal magnetic enhancements for large, young basins is an observed feature of the map, independent of any particular physical explanation.

6. Empirical model

Other post-Nectarian impact basins show evidence for demagnetization (Hertzsprung, Humorum, Moscoviense, Nectaris) and/or antipodal magnetization (Nectaris, Humboldtianum); however, these basins and antipodes are close together and in some cases overlapping (Fig. 4). To investigate superposition relationships systematically, we developed an empirical model based on the assumption that all basin-forming impacts completely demagnetize the target material within the main rim, while the largest impacts (those that create basins larger than 500 km in diameter) magnetize the antipode to a degree that depends on the basin's size and age: $B(r) = B_o(t)\exp(-\alpha r/D)\exp(D/D_I)$, where $B_o(t)$ is a time-dependent normalization (Table 1), r is radius from the antipode center, α is a scale factor, D is the diameter of the basin's main rim, and $D_I = 1200$ km is the diameter of Imbrium.

The model is constructed by starting with a uniform 1-nT surface field and sequentially applying the magnetizing and demagnetizing effects of all basin-forming impacts identified by Wilhelms (Table 1). The initial field accounts for weak, widely distributed, small-scale magnetization contrasts, which might arise from impacts earlier than those in Table 1, or from impact disruption of a global magnetized layer created at the time of crustal formation. Alternatively, the initial field could represent a relatively minor component of magnetized material that is widely distributed around the entire Moon by impacts. Whatever its origin, this field significantly improves the agreement in regions that are not antipodal to any cataloged basin.

The age profile, $B_o(t)$, could represent the history of the lunar magnetizing field as inferred from lunar sample measurements, which peaks from 3.9 to 3.6 Gyr ago and is about an order of magnitude weaker before and after (Cisowski et al., 1983), although demagnetization from many smaller impacts should be at least partly responsible for erasing the antipodal signatures of basins over time. The relatively weak magnetic signature of the Nectaris antipode compared with those of the similarly sized but younger Serenitatis and Crisium antipodes is consistent with such a history. The parameter α was adjusted to best reproduce the radial magnetic field intensity profile of the Imbrium antipodal region, yielding $\alpha = 5$. This value also provides reasonable agreement with the other large, young antipodal zones: Orientale, Serenitatis, and Crisium. The cutoff at $D = 500$ km reflects that fact that there are no antipodal magnetic field signatures for basin diameters smaller than 500 km, most notably Schrödinger, Sikorsky–Rittenhouse, and Bailly, which are all poleward of 60 N.

The resulting model largely resembles the observed map (Fig. 4), although there are significant differences. The model does not reproduce the offset of the peak magnetic field strength from the center of the Orientale antipode, nor does it account for the "bridge" of magnetic anomalies between the Orientale and Imbrium antipodal zones. Also, the pattern of magnetic highs and lows from 120° E to 80° W and poleward of 45° N, which is due to some of the oldest impacts in the model (Coulomb–Sarton, Poincaré, Mutus–Vlacq, and Australe), does not match the observations well. The signatures of these and other pre-Nectarian basins might have been obscured by impact demagnetization from the many smaller impacts that do not form basins, as well as the near-field emplacement of magnetized ejecta, neither of which were included in the model. Nevertheless, the similarity of the model and the observations, together with the clear magnetic signatures of the Imbrium and Orientale impacts, show that the effects of basin-forming impacts dominate the large-scale distribution of magnetized crust on the Moon.

7. Conclusion

We have presented a global map of lunar surface magnetic fields obtained by electron reflectometry. On small scales, the scattered distribution of magnetic anomalies and the lack of fringing fields for craters larger than 50 km in diameter indicate that crustal fields lack spatial coherence on scales larger than

~25 km, possibly as a result of impact disruption of the upper ~10 km of the crust. There is evidence for magnetized Imbrium ejecta: elongated magnetic features associated with Reiner Gamma and Rima Sirsalis, as well as magnetic anomalies correlated with Cayley deposits. On large scales, surface magnetic fields are generally stronger over highland terrain than over the maria, while the strongest fields (>40 nT) are concentrated within the antipodal zones of the four largest post-Nectarian impact basins. The Imbrium and Orientale basins themselves are regions of very weak surface fields (<0.2 nT), most likely as a result of thermal and shock demagnetization associated with those impacts. Thus, the distribution of surface magnetic fields on the Moon appears to be dominated by impact phenomena.

References

Acuña, M.H., Connerney, J.E.P., Wasilewski, P., Lin, R.P., Carlson, C.W., Curtis, D.W., Mitchell, D., Rème, H., Mazelle, C., Sauvaud, J.A., d'Uston, C., Cros, A., Medale, J.L., Bauer, S.J., Cloutier, P., Mayhew, M., Winterhalter , D., Ness, N.F., 1999. Global distribution of crustal magnetism discovered by the Mars Global Surveyor MAG/ER experiment. Science 284, 790–793.

Anderson, K.A., Lin, R.P., McGuire, R.E., McCoy, J.E., 1975. Measurement of lunar and planetary magnetic fields by reflection of low energy electrons. Space Sci. Instr. 1, 439–470.

Anderson, K.A., Lin, R.P., McGuire, R.E., McCoy, J.E., Russell, C.T., Coleman, P.J., 1977. Linear magnetization feature associated with Rima Sirsalis. Earth Planet. Sci. Lett. 34, 141–151.

Bratt, S.R., Solomon, S.C., Headm, J.W., 1985. The evolution of impact basins—Cooling, subsidence, and thermal stress. J. Geophys. Res. 90, 12415–12433.

Cashore, J., Woronow, A., 1985. A new Monte Carlo model of lunar megaregolith development. J. Geophys. Res. 90, C811–C816.

Chapman, C.R., Morrison, D., 1994. Impacts on the Earth by asteroids and comets: Assessing the hazard. Nature 367, 33–40.

Cisowski, S.M., Collinson, D.W., Runcorn, S.K., Stephenson, A., Fuller, M., 1983. A review of lunar paleointensity data and implications for the origin of lunar magnetism. J. Geophys. Res. Suppl. 88, A691–A704.

Coleman, P.J., Lichtenstein, B.R., Russell, C.T., Sharp, L.R., Schubert, G., 1972. Magnetic fields near the Moon. Proc. Lunar Sci. Conf. 3, 2271–2286.

Connerney, J.E.P., Acuña, M.H., Wasilewski, P.J., Ness, N.F., Réme, H., Mazelle, C., Vignes, D., Lin, R.P., Mitchell, D.L., Cloutier, P.A., 1999. Magnetic lineations in the ancient crust of Mars. Science 284, 794–798.

Delory, G.T., Mitchell, D.L., Halekas, J., Lin, R.P., Frey, S., 2002. Correlations between in situ and remotely sensed magnetic anomalies on the Lunar Prospector mission. In: AGU Spring Meeting Abstracts. Abstract GP42A-02.

Dyal, P., Parkin, C.W., 1972. Lunar properties from transient and steady magnetic field measurements. Moon 4, 63–87.

Fuller, M., 1974. Lunar magnetism. Rev. Geophys. Space Phys. 12, 23–70.

Fuller, M., Cisowski, S., 1987. Lunar paleomagnetism. In: Jacobs, J. (Ed.), Geomagnetism, vol. 2. Academic Press, London, pp. 307–455.

Fuller, M., Rose, F., Wasilewski, P.J., 1974. Preliminary results of an experimental study of the magnetic effects of shocking lunar soil. Moon 9, 57–61.

Halekas, J.S., Mitchell, D.L., Lin, R.P., Frey, S., Hood, L.L., Acuña, M.H., Binder, A.B., 2001. Mapping of crustal magnetic anomalies on the lunar near side by the Lunar Prospector Electron Reflectometer. J. Geophys. Res. 106, 27841–27852.

Halekas, J., Mitchell, D.L., Lin, R.P., Hood, L.L., Acuña, M.H., Binder, A.B., 2002a. Demagnetization signatures of lunar impact craters. Geophys. Res. Lett. 29, doi:10.1029/2001GL013924. 23-1.

Halekas, J., Mitchell, D.L., Lin, R.P., Hood, L.L., Acuña, M.H., Binder, A.B., 2002b. Evidence for negative charging of the lunar surface in shadow. Geophys. Res. Lett. 29, doi:10.1029/2001GL014428. 77-1.

Hood, L.L., 1986. Geophysical constraints on the lunar interior. In: Hartmann, W.K., Phillips, R.J., Tayor, G.J. (Eds.), Origin of the Moon. Lunar and Planetary Institute, Houston, TX, pp. 361–410.

Hood, L.L., Artemieva, N.A., 2008. Antipodal effects of lunar basin-forming impacts: Initial 3D simulations and comparisons with observations. Icarus 193, 485–502.

Hood, L.L., Huang, Z., 1991. Formation of magnetic anomalies antipodal to lunar impact basins—Two-dimensional model calculations. J. Geophys. Res. 96, 9837–9846.

Hood, L.L., Vickery, A., 1984. Magnetic field amplification and generation in hypervelocity meteoroid impacts with application to lunar paleomagnetism. J. Geophys. Res. 89, C211–C223.

Hood, L.L., Coleman, P.J., Wilhelms, D.E., 1979. Lunar nearside magnetic anomalies. Proc. Lunar Sci. Conf. 10, 2235–2257.

Hood, L.L., Zakharian, A., Halekas, J., Mitchell, D.L., Lin, R.P., Acuña, M.H., Binder, A.B., 2001. Initial mapping and interpretation of lunar crustal magnetic anomalies using Lunar Prospector magnetometer data. J. Geophys. Res. 106, 27825–27840.

Hörz, F., Gibbons, R.V., Hill, R.E., Gault, D.E., 1976. Large scale cratering of the lunar highlands: Some Monte Carlo model considerations. Proc. Lunar Sci. Conf. 7, 2931–2945.

Lin, R.P., 1979. Constraints on the origins of lunar magnetism from electron reflection measurements of surface magnetic fields. Phys. Earth Planet. Int. 20, 271–280.

Lin, R.P., Anderson, K.A., Bush, R., McGuire, R.E., McCoy, J.E., 1976. Lunar surface remanent magnetic fields detected by the electron reflection method. Proc. Lunar Sci. Conf. 7, 2691–2703.

Lin, R.P., Anderson, K.A., Hood, L.L., 1988. Lunar surface magnetic field concentrations antipodal to young large impact basins. Icarus 74, 529–541.

Lin, R.P., Mitchell, D.L., Curtis, D.W., Anderson, K.A., Carlson, C.W., McFadden, J., Acuña, M.H., Hood, L.L., Binder, A.B., 1998. Lunar surface magnetic fields and their interaction with the solar wind: Results from Lunar Prospector. Science 281, 1480–1484.

Lucey, P., Korotev, R.L., Gillis, J.J., Taylor, L.A., Lawrence, D., Campbell, B.A., Elphic, R., Feldman, B., Hood, L.L., Hunten, D., Mendillo, M., Noble, S., Papike, J.J., Reedy, R.C., Lawson, S., Prettyman, T., Gasnault, O., Maurice, S., 2006. Understanding the lunar surface and space–Moon interactions. Rev. Mineral. Geochem. 60, 83–219.

Nagata, T., Fisher, R.M., Schwerer, F.C., Fuller, M.D., Dunn, J.R., 1972. Rock magnetism of the Apollo 14 and 15 materials. Proc. Lunar Sci. Conf. 3, 2423–2447.

Orphal, D.L., Borden, W.F., Larson, S.A., Schultz, P.H., 1980. Impact melt generation and transport. Proc. Lunar Sci. Conf. 11, 2309–2323.

Pittman III, W.C., Heirtzler, J.R., 1966. Magnetic anomalies over the Pacific–Antarctic ridge. Science 154, 1164–1166.

Russell, C.T., Coleman, P.J., Lichtenstein, B.R., Schubert, G., 1978. The permanent and induced magnetic dipole moment of the Moon. Proc. Lunar Sci. Conf. 5, 2747–2760.

Srnka, L.J., Hoyt, J.L., Harvey, J.V.S., McCoy, J.E., 1979. A study of the Rima Sirsalis lunar magnetic anomaly. Phys. Earth Planet. Int. 20, 281–290.

Stoffler, D., Ryder, G., 2001. Stratigraphy and isotope ages of lunar geologic units: Chronological standard for the inner Solar System. Space Sci. Rev. 96, 9–54.

Toksöz, M.N., Dainty, A.M., Solomon, S.C., Anderson, K.R., 1973. Velocity structure and evolution of the Moon. Proc. Lunar Sci. Conf. 4, 2529–2547.

Vine, F.J., Matthews, D.H., 1963. Magnetic anomalies over oceanic ridges. Nature 199, 947–949.

Vine, F.J., Wilson, J.T., 1965. Magnetic anomalies over a young oceanic ridge off Vancouver Island. Science 150, 485–489.

Watts, A.W., Greeley, R., Melosh, H.J., 1991. The formation of terrains antipodal to major impacts. Icarus 93, 159–168.

Wieczorek, M.A., Jolliff, B.L., Khan, A., Pritchard, M.E., Weiss, B.P., Williams, J.G., Hood, L.L., Righter, K., Neal, C.R., Shearer, C.K., McCallum, I.S., Tompkins, S., Hawke, B.R., Peterson, C., Gillis, J.J., Bussey, B., 2006. The constitution and structure of the lunar interior. Rev. Mineral. Geochem. 60, 221–364.

Wilhelms, D.E., 1984. Moon. In: The Geology of the Terrestrial Planets. NASA SP-469. NASA, Washington, DC, pp. 107–205.

Williams, K.K., Zuber, M.T., 1998. Measurement and analysis of lunar basin depths from Clementine altimetry. Icarus 131, 107–122.